A stochastic spatio-temporal (SST) model to study cell-to-cell variability in HIV-1 infection

Zhang Cheng*, Alexander Hoffmann*

Department of Microbiology, Immunology, and Molecular Genetics (MIMG), and Institute for Quantitative and Computational Biosciences (QCB), UC, Los Angeles, CA 92093, United States

HIGHLIGHTS

- We developed a stochastic intracellular mathematical model of HIV replication.
- The model includes spatial microtubule transport of viral components.
- The model can simulate single round infections and viral fates.
- The model predicts that vRNA decay and RT are critical determinants of integration.

GRAPHICAL ABSTRACT
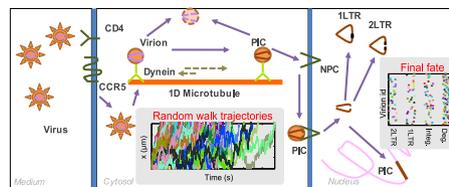
ABSTRACT

Although HIV viremia in infected patients proceeds in a manner that may be accounted for by deterministic mathematical models, single virus-cell encounters following initial HIV exposure result in a variety of outcomes, only one of which results in a productive infection. The development of single molecule tracking techniques in living cells allows studies of intracellular transport of HIV, but it remains less clear what its impact may be on viral integration efficiency. Here, we present a stochastic intracellular mathematical model of HIV replication that incorporates microtubule transport of viral components. Using this model, we could study single round infections and observe how viruses entering cells reach one of three potential fates – degradation of the viral RNA genome, formation of LTR circles, or successful integration and establishment of a provirus. Our model predicts global trafficking properties, such as the probability and the mean time for a HIV viral particle to reach the nuclear pore. Interestingly, our model predicts that trafficking determines neither the probability or time of provirus establishment – instead, they are a function of vRNA degradation and reverse transcription reactions. Thus, our spatio-temporal model provides novel insights into the HIV infection process and may constitute a useful tool for the identification of promising drug targets.

© 2016 Elsevier Ltd. All rights reserved.

1. Introduction

Human immunodeficiency virus (HIV) is an enveloped single-stranded RNA virus. The most common and natural route of HIV infection is via sexual mucosal transmission. There are different time scales associated with the infection process. At the early stages (usually in the first few hours post infection), HIV will cross the mucosal barrier and only a small number of cells are successfully infected; these constitute the seed or founder population, which after several days start production of new virus. Within the first week, lymphatic tissue reservoirs will trigger the conversion to the seropositive infection state. Thus, the early phases of HIV exposure and infection are of critical importance, and they are believed to provide a window of opportunity that determines sero-conversion, as well as – if sero-conversion cannot be prevented – the viral set point that determines collapse and

* Corresponding authors.
  E-mail addresses: z2cheng@ucla.edu (Z. Cheng),
ahoffmann@ucla.edu (A. Hoffmann).

amplification processes (Haase, 2010). Thus early phase infection events are critical in determining the fate of the exposed individual. Here, we present a mathematical framework to address the stochastic nature of the early phases of the HIV life cycle, namely from docking to establishment of a provirus.

The HIV life cycle begins when the envelope (Env) glycoprotein (gp120) binds to the host surface receptor (CD4) and co-receptor (CCR5 or CXCR4). Then the virion either fuses with host cell membranes in a pH-independent manner (Stein et al., 1987) or via an alternative endocytic pathway (Miyauchi et al., 2009). Once inside the cell, the virus is transported across the actin layer and undergoes uncoating to generate the viral reverse transcription complex (RTC), which comprises the diploid viral RNA genome, tRNALys primer, RT, IN, MA, nucleocapsid (NC), viral protein R (Vpr) and various host proteins. Once the RTC reaches close to nuclear pore complex (NPC) via microtubule, they will dock to NPC and undergoes DNA-Flag-dependent maturation, forming a pre-integration complex (PIC) (Arhel et al., 2007). Then the PIC translocate through the nuclear pore to get inside of the nucleus. In the nucleus, the PIC can either integrate into the host chromatin or circularizes into 1- or 2 LTR circles.

A large portion of the early HIV life cycle is taken up by transcellular transport that moves the virus from the plasma membrane to the nuclear pore (Brandenburg and Zhuang, 2007). It is found that after fusion, the virus will go through three kinetically distinguishable directed movements until it reaches the nuclear surface. It first travels across one actin layer with a random diffusion, then binds to the microtubule and trafficks along it until reaching the proximal of the nuclei, where it has to cross another actin layer to reach the NPC on the nuclear membrane (Arhel et al., 2006; McDonald et al., 2002). How trafficking relates to infectivity is an important question.

Mathematical modeling has been applied at different levels of HIV infection rendering quantitative insights. Perhaps, the most established models are those of viral dynamics within patients (Perelson, 2002).They focus on the dynamics of virion numbers and numbers of different cell types during the HIV infection and AIDS development. At the molecular level, molecular dynamic simulations were used to study kinetic mechanisms of the HIV-1 viral protein conformational transitions (Deng et al., 2011). At the intracellular level, a detailed deterministic model was proposed by John Yin's group (Reddy and Yin, 1999), with other simplified models for different focus. Weinberger developed a small stochastic model to study the HIV gene expression and replication (Weinberger et al., 2005). Kim and Yin proposed a model to study different splicing products during HIV replication (Kim and Yin, 2005). Later, Althaus and De Boer presented a combination of the models developed by Weinberger and Reddy to study the relationship between viral transcription and the viral load during drug therapy (Althaus and De Boer, 2010). These models account for mechanistic details about HIV intracellular replication, though they exclude intracellular transport of viral components. Dinh developed such models to study adenoviral vectors transportation (Dinh et al., 2005; Dinh et al., 2007) in the context of gene therapy, but how trafficking and biochemical reactions combine to give rise to HIV replication remains elusive. Here we present a model that couples reactions with transport and provides a more accurate description of HIV replication in agreement with recent experimental observations.

An infection may be initiated by a single virus particle that delivers its genome, a single molecule of RNA, to its host cell. Under such conditions, the inherent fluctuations in the levels of viral constituents may yield qualitatively different behavior (Srivastava et al., 2002). Deterministic models that describe the expected progress of the infection cannot be employed to predict the probability of infection establishment at the primary stage (Khalili and Armaou, 2008). In this study, we integrate the HIV transport with basic HIV life cycle model and establish a stochastic spatio-temporal model to study early HIV infection. The model can

track each infected single virus's life cycle. Three different fates of the virus can be recapitulated by the model. We also used the model to study the effects of each parameter on the integration fraction and time to integration.

2. Methods

We first developed an ODE model to derive kinetic parameters for key reactions in the HIV life cycle from recent experimental results of a fine-grained timecourse (Mohammadi et al., 2013). We then developed the SST model (Fig. 1A) using those parameters. The overall model development process is shown in Fig. 1B.

2.1. An ODE model to derive parameters

As the *in vitro* infection experiment (Mohammadi et al., 2013) VSVg-pseudo-typed virus was used, the receptor and co-receptor binding, the fusion and uncoating parameters are not relevant to the *in vivo* HIV infection. We therefore developed a simplified ODE model (Fig. S1) to account for the experimental measurement and derive the useful parameters for the SST model.

$$\frac{dV}{dt} = \theta_1 \cdot \theta_2 \cdot e^{-\theta_2 t} - \theta_{11} \cdot V \tag{1}$$

$$\frac{dERT}{dt} = \theta_{11} \cdot V - \theta_3 \cdot ERT \tag{2}$$

$$\frac{dD}{dt} = \theta_3 \cdot ERT(t - \theta_{12}) - (\theta_4 + \theta_5 + \theta_6 + \theta_7) \cdot D \tag{3}$$

$$\frac{dL_1}{dt} = \theta_7 \cdot D - \theta_8 \cdot L_1 \tag{4}$$

$$\frac{dL_2}{dt} = \theta_6 \cdot D - \theta_9 \cdot L_2 \tag{5}$$

$$\frac{dI}{dt} = \theta_5 \cdot D - \theta_{10} \cdot I \tag{6}$$

In this model, V is the virion concentration inside the cell; ERT-early reversible transcription product, D-linear cDNA, L1–1 LTR circle; L2–2LTR circle. I – integrated provirion.

The virion internalization is assumed to be a first order process with rate constant θ_2 and the initial virus concentration in the media is θ_1. Then the outside virion concentration V_o can be described by ODE: $dV_o/dt = -\theta_2 V_o$ with initial concentration θ_1. So $V_o = \theta_1 \, exp(-\theta_2 t)$, and the internalization flux in Eq. (1): $\theta_2 V_o = \theta_1 \theta_2 \, exp(-\theta_2 t)$. The full description of the parameters in the model can be found in Fig. S1C. The experimental data (Fig. 1A and Fig. S2 from (Mohammadi et al., 2013)) were measured by qPCR and normalized to each species' own specific value at 24 h. To match such kinds experimental data, scaling parameters have to be introduced in the model (see θ_{13-16} in Fig. S1C).

To fit the experimental data, we used RMSD between simulation and data as the objective function and employed nonlinear least-squares solver -'lsqnonlin' function from Matlab to run the optimization. As 'lsqnonlin' can only find the local minimum, we supplied it with 10^6 initial parameter values in the parameter space (10^{-2} to 10^2 for non-scale parameters and 10^{-5} to 10^{-1} for the scaling parameter). We recorded the best solution and the 95% confidence interval for each parameter defined by the boundary of changing RMSD 5% as well.

2.2. The SST model

The model diagram and reactions are shown in Fig. 1A and Table 1. The model consists of three parts. The first part includes binding and unbinding to the CD4 receptor and co-receptor (CCR5 in this study),
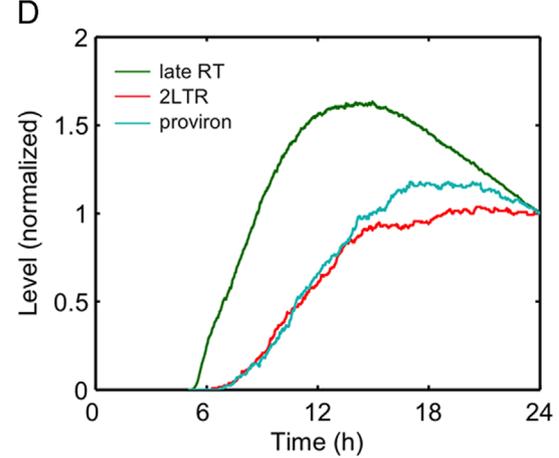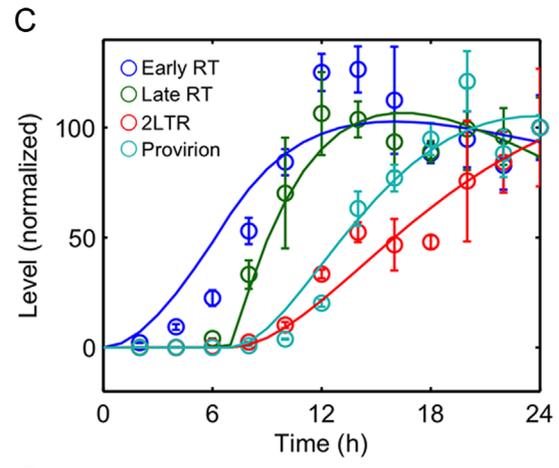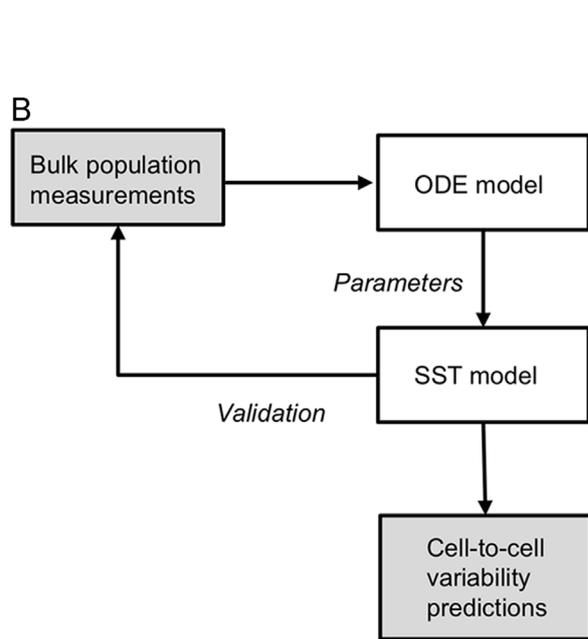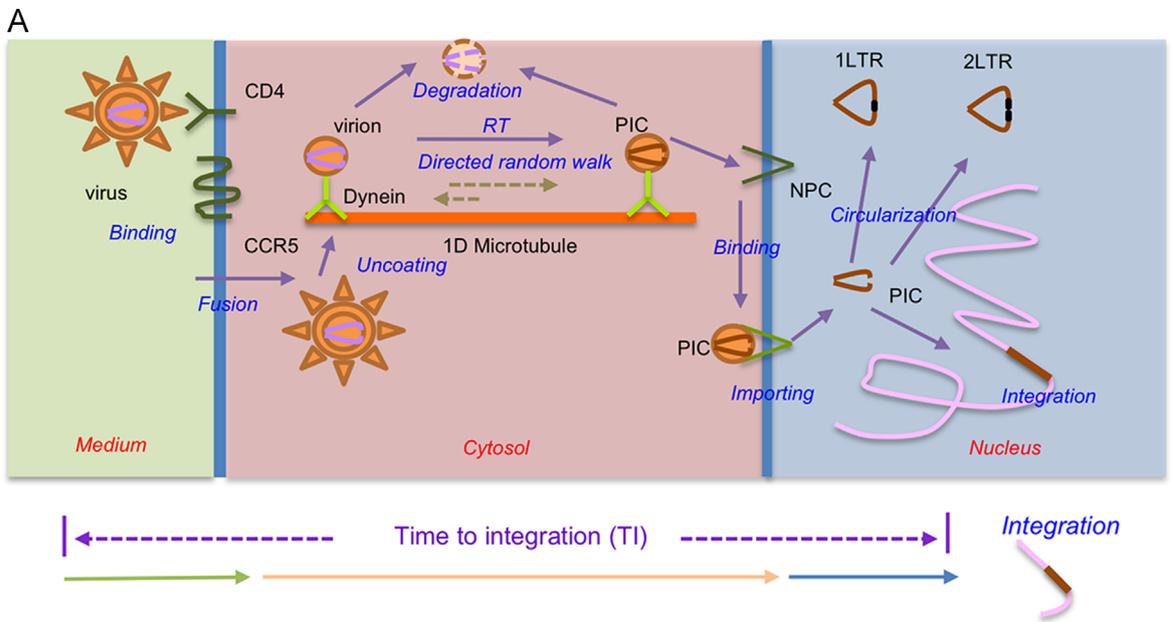
Fig. 1. Model overview. (A) Stochastic spatio-temporal (SST) model diagram and illustration of time to integration (TI). (B) Flowchart of integrating ODE and SST models. Bulk population measurements are taken from Mohammadi et al. (Mohammadi et al., 2013). (C) ODE model's simulation (lines, upper panel) is compared with experimental data (circles, upper panel). (D) The average time courses predicted from the SST model by simulating 100,000 infections. The levels are normalized to the values at 24-hour post infection for each component.

and fusion. The second part consists of the reaction describing uncoating, degradation, reverse transcription, nuclear core complex binding and nuclear importing, along with a spatial transportation. The last part is the fate decision module: 1LTR or 2LTR circularization and integration. The life cycle steps are modeled as chemical reactions by using Gillespie method (Gillespie, 1977), while actin transport is modeled by a modified method from Dinh et al. (2005). As a result, the spatial and temporal parts of the model can be modeled in a uniformed stochastic framework enabling studies of the variability of infection fates.

Table 1
Model reactions and parameters.

#	Reactions	Description	Value	References
Set 1	$(Virion)_{free}+(CD4)_{pm} => (Virion:CD4)_{pm}$	HIV binds to the receptor	$4.03e+6\,M^{-1}min^{-1}$	Table 3 in Myszka et al. (2000)
	$(Virion:CD4)_{pm} => (Virion)_{free}+(CD4)_{pm}$	HIV unbinds from the receptor	$0.09\,min^{-1}$	Table 3 in Myszka et al. (2000)
	$(CCR5)_{pm}+(Virion:CD4)_{pm} => (Virion:CD4:CCR5)_{pm}$	HIV:receptor complex binds to the co-receptor	$5.4e+6\,M^{-1}\,min^{-1}$	Doranz et al. (1999)
	$(Virion:CD4:CCR5)_{pm} => (CCR5)_{pm}+(Virion:CD4)_{pm}$	HIV:receptor complex unbinds from the co-receptor	$log(2)/32\,min^{-1}$	Doranz et al. (1999)
	$(Virion:CD4:CCR5)_{pm} => (Virion)_{peripheral}+(CD4)_{pm}+(CCR5)_{pm}$	Fusion	$log(2)/20\,min^{-1}$	Hulme et al. (2011), Raviv et al. (2002)
	$(Virion)_{peripheral} => (RTC)_{peripheral}$	Uncoating	$log(2)/23\,min^{-1}$	Table 1 in Hulme et al. (2011)
Set 2	(RTC) random walk along microtubule (virus trafficking from $x=0$ to $x=$length of microtubule)	Microtubule length	$20\,\mu m$	See the scale bar of Fig. 1 in McDonald et al. (2002)
		Average velocity of directional movements in both direction	$6\,\mu m/min$	Arhel et al. (2006), Arhel et al. (2007)
		First order rate constants of characterizing particle's transition to anterograde movement state	$1.1\,min^{-1}$	Adjusted to fit the ODE model
		First order rate constants of characterizing particle's transition to retrograde movement state	$1\,min^{-1}$	Adjusted to fit the ODE model
		First order rate constants of characterizing particle's transition to static state	$1\,min^{-1}$	Adjusted to fit the ODE model
	$(RTC)(x) => (PIC)(x)$	Reverse transcription	$0.0024\,min^{-1}$	From ODE model (theta3)
	$(RTC)(x) =>$	Degradation of RTC (virial RNA)	$0.0033\,min^{-1}$	$0.2\,h^{-1}$ (Table I in Reddy and Yin (1999))
	$(PIC)(x) =>$	Degradation of PIC (virial DNA on the microtubule or in the cytoplasm or in the nuclears)	$0.017\,min^{-1}$	From ODE model (theta 4)
Set 3	$(PIC)_{perinuc} => (PIC)_{nuc}$	Nuclear import	$0.002\,min^{-1}$	Reddy and Yin (1999)
	$(PIC)_{nuc} => (Provirion)_{int}$	Integration	$0.00053\,min^{-1}$	From ODE model (theta 5)
	$(PIC)_{nuc} => (2LTRcir)_{nuc}$	Circularization	$0.00051\,min^{-1}$	From ODE model (theta 6)
	$(PIC)_{nuc} => (1LTRcir)_{nuc}$	Circularization	$0.015\,min^{-1}$	From ODE model (theta 7)
	$(2LTR)_{nuc} =>$	Degradation of 2LTR circles	$0.00065\,min^{-1}$	From ODE model (theta 9)
	$(1LTR)_{nuc} =>$	Degradation of 1LTR circles	$0.13\,min^{-1}$	From ODE model (theta 8)
	$(Provirion)_{nuc} =>$	Degradation of Provirion	$0.00097\,min^{-1}$	Equal to the CD4 cell death rate (Ho et al., 1995)
		Initial cell volume (V_0)	$1e-12\,L$	ID 106314 in Bionumber database

Table 2
Initial states.

#	Biophysical States		Values	Location	Sources
1	$(Virion)_{free}$	Virions in the medium	1 virion/cell	Mucosal surface	Assumed
2	$(CD4)_{pm}$	CD4 on the plasma membrane	46000	Plasma membrane	Poncelet et al. (1991)
3	$(CCR5)_{pm}$	CCR5 on the plasma membrane	10000	Plasma membrane	Reynes et al. (2000)
4	$(Virion:CD4)_{pm}$	Virion:CD4 complex on the Plasma membrane	0	Plasma membrane	Assumed
5	$(Virion:CD4:CCR5)_{pm}$	Virion:CD4:CCR5 complex on the Plasma membrane	0	Plasma membrane	Assumed
6	$(Virion)_{peripheral}$	Fused virion	0	Cytoplasm	Assumed
7	$(RTC)_{peripheral}$ or $(RTC)(x=0)$	Reverse transcription complex (uncoated form)	0	Cytoplasm	Assumed
8	$(RTC)(x)$ $(0 <= x <= len_{MT})$	Microtubule binding state	0	Cytoplasm (microtubule)	Assumed
9	$(PIC)(x)$ $(0 < x <= len_{MT})$	Docked pre-integration complex	0	Cytoplasm (microtubule)	Assumed
10	$(PIC)_{perinuc}$ or $(PIC)(x=len_{MT})$	Docked pre-integration complex	0	Perinuclear area	Assumed
11	$(PIC)_{nuc}$	Imported pre-integration complex	0	Nucleus	Assumed
12	$(1LTR)_{nuc}$	1LTR circle	0	Nucleus	Assumed
13	$(2LTR)_{nuc}$	2LTR circle	0	Nucleus	Assumed
13	$(Provirion)_{int}$	Integrated provirion	0	Nucleus	Assumed
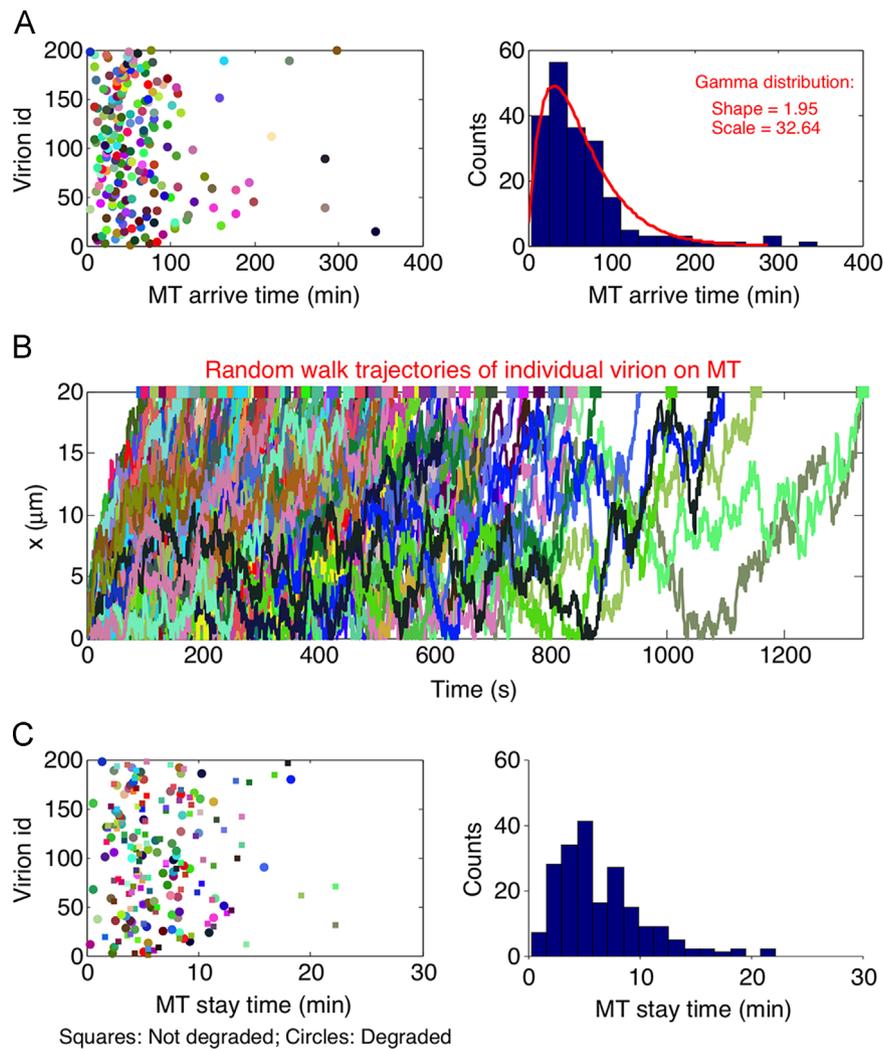
Fig. 2. *SST model tracks viral infections individually.* (A) Microtubule (MT) arrive time statistics. Left: scatter plot between virion id (1–200, color-coded) and MT arrive time; right: histogram of MT arrive time of these 200 infections. (B) Trafficking trajectories along the microtubule for each virion. The x-axis is the trafficking time and y-axis is the displacement along the MT. The virons that successfully arrived the end of MT are labeled by squares. The same colors as (A) are used to identify virus. (C) Statistics of the trafficking time. Left: scatter plot between virion id and MT stay time; right: histogram of MT stay time. The squares represent the degraded virions and the circles represent the ones not degrade.

Details about the reactions, the parameters and initial states can be found in Tables 1 and 2, with references for each parameter. Below we describe the details of the second part of the model, because the spatial and temporal reactions are mixed at this stage.

2.3. Intracellular trafficking

We focused here on the trafficking along the microtubule, assuming that other motions make only minor contributions to the
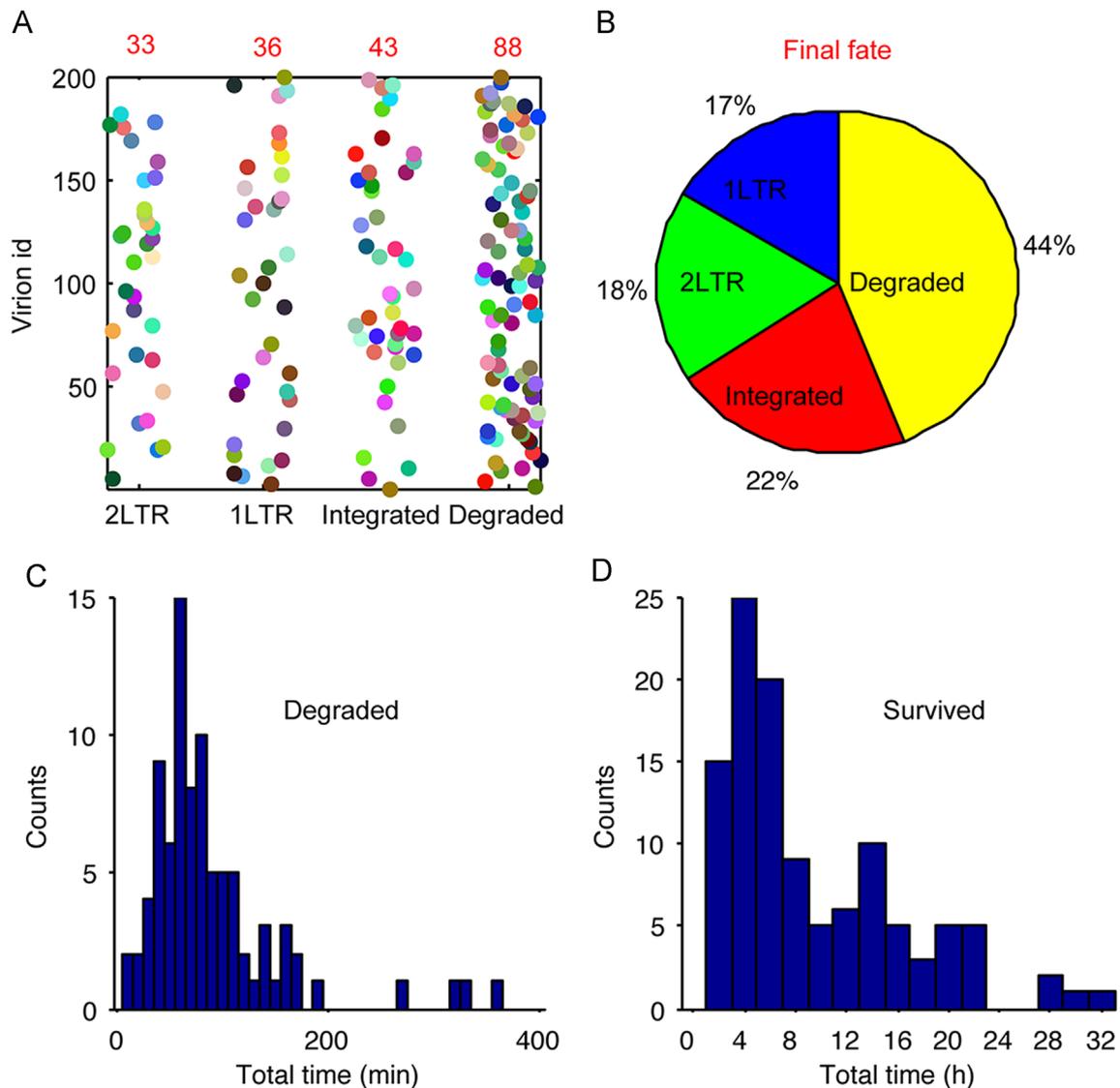
Fig. 3. *SST model tracks 200 infections individually (final states).* Final fate distribution of all virions (A, same color-coding as Fig. 2; the number of virions in each catalog is shown in red) and the percentages of fates (B). Histogram of fate decision time for degraded (C) and survived (D) virions. Survived population includes the ones formed 2LTR, 1LTR and proviron.

relevant intracellular transport of the virion. We assumed transport to begin as soon as the virus uncoated. The viral transportation along the microtubule is modeled as a one-dimensional random walk. At a given point in time, each virus particle occupies one of the three transport states: forwards move, backwards move or stall (Dinh et al., 2005). The motion state and the time interval to make a state transition are determined by random numbers akin to the Gillespie method, and the virus will be trafficking back and forth as the simulation goes on. Once the virus reaches the end of the microtubule, the transportation process will terminate, and the infection progresses towards the next step, i.e. binding to the NPC. The model may be used to record the trajectory of each virus trafficking long the microtubule. To simplify the simulation process we assume that different viruses do not interfere with each other in the microtubule. At the population level this assumption holds true when no cell is infected by more than one virus. The model results can be considered as the outcome of a single round of infection.

2.4. Degradation and reverse transcription during the transport

It is reported that during the transportation, the virion can either go through reverse transcription to form a reverse transcription complex (RTC) and then the pre-integration complex (PIC) via reverse transcription or is degraded by cellular mechanisms (Anderson et al., 2006). In order to model this, we tracked these two reactions in parallel with the viral particle's trafficking (Fig. S2). In practice, we first simulate viral trafficking and obtain a time of arrival. Then, we simulate degradation and reverse transcription, and check if either occurred within the time of arrival (see Fig. S2). If degradation did occur, the model provides information about the location where it gets degraded. Note that the degradation can even happen when the virion has reached the end of the microtubule, as long as reverse transcription has not occurred. The reverse transcription and degradation are the only reactions that can occur during transport.
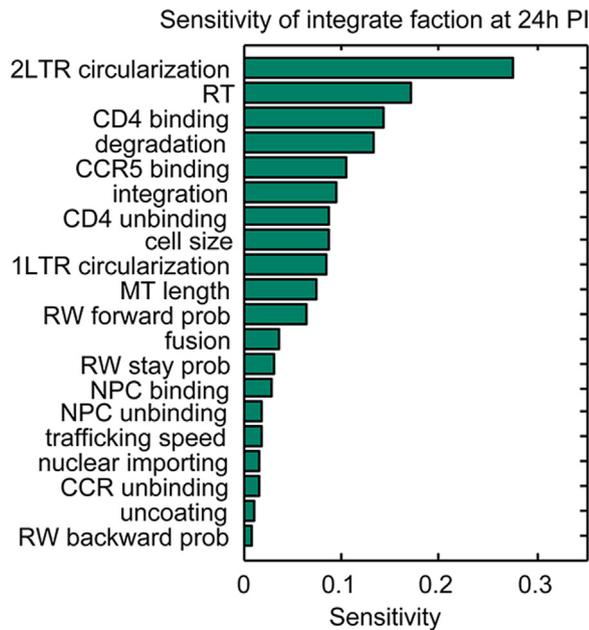
Fig. 4. *Sensitivity analysis of the integration fraction at* 24 h *post infection* (f_{24pi})*. The sensitivities are sorted from high to low for steps in the SST model.*

2.5. Virion fates

There are three different fates of HIV in this model: degraded (killed by the cell), LTR circles (non-productive), or integrated provirus (productive infection). Here, we study the integration fraction and the time to integration (TI), which is important because it measures how soon a latency state can be established. A short TI can also lower the chance to trigger the host immune system.

2.6. Sensitivity analysis

To quantify how the steps in HIV replication cycle affect the infection, we calculated the sensitivity of infection fraction at 24-hour post infection (f_{24hpi}). The sensitivity of parameter p_j was defined as the rate of change in f_{24hpi} divided by the rate of change in the parameter value.

$$S_j = \frac{\frac{\partial f_{24hpi}}{f_{24hpi}}}{\frac{\partial p_j}{p_j}} = \frac{\partial \ln f_{24hpi}}{\partial \ln p_j} \tag{7}$$

The effect of a 2% change of each parameter value was considered here. For the SST model, the f_{24hpi} was calculated by simulating the model 5000 times to get the fraction of the integration achieved at 24 h post infection. For the ode model, the f_{24hpi} was directly calculated by one simulation.

3. Results and discussion

3.1. Model validation

With the development of PCR primers specific for viral intermediates, the HIV replication dynamics have been intensively studied (Brussel and Sonigo, 2003; Butler et al., 2001; Butler et al., 2002; Mohammadi et al., 2013). Here we used the recent data from Mohammadi et al. (2013), where the early RT, late RT, 2LTR circles and the integrated proviron are measured every 2 h in the first 24 h post infection (h.p.i.). Because the infection in the experiment used a VSVg pseudo-typed virus, the receptor and co-
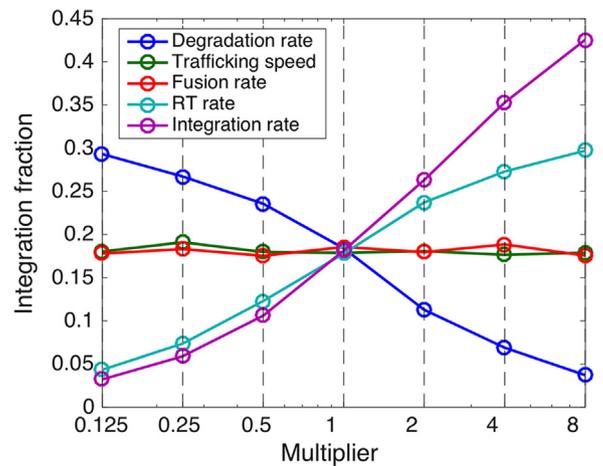
Fig. 5. *Integration fraction is a function of several key parameters*. *The x-axis is the multiplier and y-axis is the integration fraction in 5000 simulations of infection.*

receptor binding, the fusion and uncoating information cannot be extracted from the data and only a fraction of the parameters are adjusted by the ODE model's value (see Supplemental tables). Other parameters of the SST are from the literature.

After obtaining a reasonable fit of the ODE model with the data (Fig. 1C), we then ran the SST model 100,000 times to mimic a corresponding number of infections and got the average profiles. It turned out that average dynamics of the SST model were overall faster than the experimental data by about 3 h. This was because the SST model simulations begin with CD4 receptor docking, ignoring the time taken by virus diffusing to the T cell surface. After adjusting this initial time difference, the SST model successfully recapitulated the experimental observations (Fig. 1C and D): 1) The late RTC increased faster than the 2LTR, and provirion and reached a peak around 12 h.p.i. 2) The provirion accumulated a little slower than the 2LTR. Following successful parameterization of the SST model to population measurements, and we then explored cell-to-cell variability, which remains experimentally much more challenging.

3.2. Tracking each virion's state and fate

The model can track the state of each virion. We studied a small population of 200 viruses infecting an equal number of CD4 T cell and assumed a synchronized infection. We first focused on the heterogeneous timing of three HIV infection phases.

The first part of the model was examined by studying how long it will take for each virus to fuse to the cell and be bound to microtubules (Fig. 2A). We marked each infection by a unique color. The distribution for time taken for this part matches a gamma distribution, which is the consequence of multiple steps before the virion reaches the microtubule. At this stage, no viral degradation was considered.

As soon as the virion reaches the microtubule, trafficking may begin. The model then begins to record the trajectory of each virion along the microtubule (Fig. 2B and C). Each trajectory is different. Some viruses may reach the end of the microtubule within 60s, but others may not complete the journey within the 1200s time window. The simulated trajectories mimic the 1D random work towards an absorbing boundary at the nuclear membrane. The statistics of the time that each virus spends on the microtubule is plotted in Fig. 2C in two ways: The left panel shows how long each virus stays and its final fate (with squares indicating surviving and circles indicating degraded virions); the right panel shows the histogram of the MT stay time, i.e. trafficking time.
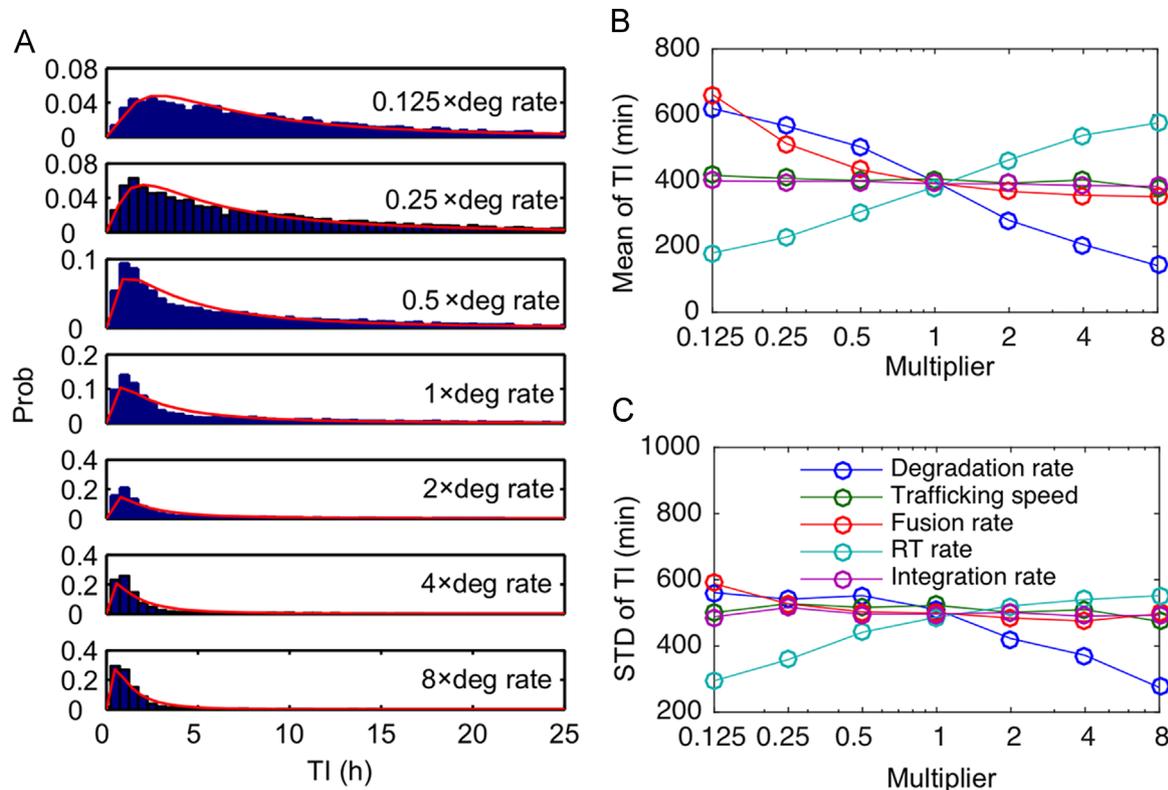
Fig. 6. *Time to integration (TI) distribution is a function of the degradation rate.* (A) Histogram of TI in 5000 infections in different degradation rates. Red lines are log-normal distribution fits. Mean (B) and standard deviation (C) of TI distribution vs. the multiplier.
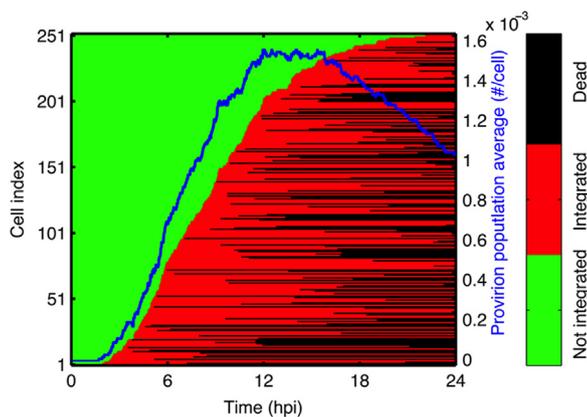
Fig. 7. *Provirion dynamics at single cell resolution.* The switching dynamics in single cells for those viruses that successfully integrated into the host genome during 24 h.p.i. The state of the infection is color-coded. Green is not integrated; red is integrated; and black is dead of the host cell. The blue line is the population average of provirion dynamics.

After reaching the end of microtubule, the virus binds the NPC and is internalized into the nucleus. Fig. 3 summarizes the fates of the viral population. Among the 200 viruses, the majority is degraded during transport (44%, Fig. 3A and B). The surviving viruses form 1LTR, 2LTR circles and provirions in similar proportions (17%, 18% and 22% respectively). We also compared the lifetime of the degraded viruses versus the survivors (Fig. 3C and D). As expected, the degraded sub-population has a shorter and tightly distributed lifetime with mean about 100 min. In contrast, the survival population has a broader distribution with a mean 4 h. The higher variability viral survivors may be due to a mixture of three different fates ones (1LTR, 2LTR and provirus).
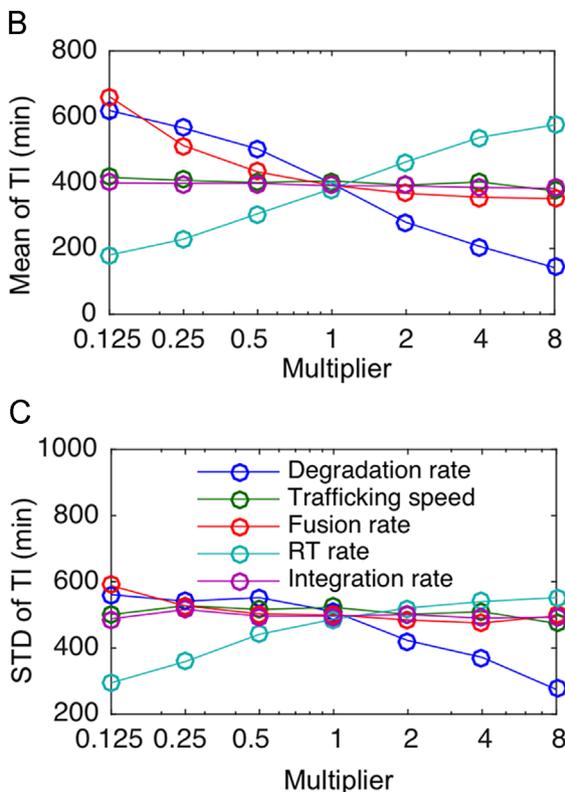
3.3. Reactions critical for HIV provirus integration

In order to address which steps are critical in the infection, we employed sensitivity analysis (Fig. 4) (Stelling et al., 2004). The subject of the sensitivity analysis is the integration fraction at 24 h. p.i.(f_{24hpi}). We chose 24 h because it is a typical cell cycle period. We perturbed each parameter 2% to see how f_{24hpi} changes. The most sensitive parameter is the 2LTR circularization rate; this may be due to the competition between circularization and integration. Reverse transcription and degradation are also sensitive, but the least sensitive parameter is the random walk probability constant. Note that the analysis here is based on a small perturbation around the original value, and so it only reflects the local sensitivity.

In order to see effects of larger perturbations, we chose five reactions, which are potential drug targets, and used larger multiplier (1/8 to 8 fold) perturbations to see how they affect the integration fraction (Fig. 5). The integration fraction here is calculated by simulating 5000 distinct infections to ensure robust statistics. It is calculated as the fraction of infected virions, which finally is successfully integrated into the host genome. The fusion reaction only contributes to the time when the virus enters the cell and does not affect the final fate of the virion. Thus the integration fraction is not sensitive to the fusion reaction.

After the virion has entered the cell, the genomic vRNA may undergo 3 alternate fates: degradation of the vRNA, integration of the cDNA, or formation of LTR circles. Thus the reactions of degradation of vRNA, reverse transcription (vDNA is not subject to degradation), or integration control the integration fraction. Interestingly, the trafficking does not contribute to the fate decision; it only determines whether degradation or RT is happening in the microtubule or at the end of microtubule.

As reverse transcription and degradation are competing processes, they have opposite effects on the integration fraction. An

increase of the degradation rate lowers the chance of integration, as does a reduction in the reverse transcription rate. A sensitivity analysis for the ODE model demonstrated that for the 11 common parameters the results are consistent with the SST model (Fig. S3).

Our analysis indicates that the degradation and the reverse transcription are key steps contributing to the infection efficiency. Interestingly, the macrophage, which shows resistance to CXCR4-ultilizing (X4) strains of HIV due to a low CXCR4 expression level (Berger et al., 1999), can be infected after increasing RT efficiency by treatment of exogenous nucleosides (Ana Sanchez et al., personal communication). This shows that enhancing RT efficiency can greatly increase the infection efficiency, validating one of our predictions.

3.4. Reactions critical for the time to integration

Next we focused on the time taken to proviral integration (TI), which measures how soon a provirus is established. A short TI may minimize the chance of triggering the host immune system via cytoplasmic RNA and DNA sensors. Since each virus-cell encounter is different, the TI actually is different for each infection and we consider here its distribution. This distribution appears to be log-normal (Fig. 6A). Interestingly, as the degradation rate is slowed, TI is longer and also more widely distributed (also can be seen from the blue lines in Fig. 6B and C). This is presumably because a slower degradation rate allows more slowly reverse transcribing virions to reach the nuclear membrane. Although we showed in the previous section that a slowing of the degradation rate increases the fraction of successfully established proviruses (Fig. 5), we suggest here that the concomitant increase in TI may render virions more likely to trigger host immune responses, which in turn may reduce their ability to establish a productive infection. Thus, our results suggest that the susceptibility of the viral genomic RNA for degradation is subject to competing selective evolutionary pressures: a long half-life favors integration efficacy, but a short half-life may be critical for evading cytoplasmic pathogen sensors that may trigger an innate immune response.

Similar conclusions may be drawn from our results of the altering the reverse transcriptase reaction: although decreased reverse transcription efficacy reduces integration effectiveness it also reduces the mean time to integration (Fig. 6B) and thus the risk of immune detection. Thus one potential effect of therapeutic compounds that inhibit reverse transcription may be a reduction in the effectiveness of the innate immune response.

TI is a measure of how long it will take a virion to successfully integrate into the host cell. Thus, unlike the integration fraction, TI depends on the fusion rate but not the integration rate. The fusion rate determines how long it takes for a bound virion to enter the host cell. The integration rate determines the possibility of integration as opposed to circularization, and it does not contribute to TI. Interestingly the trafficking speed also has little impact on the time to integration, confirming that reverse transcription is largely rate limiting for allowing integration.

3.5. Provirion fate transition dynamics

The stochastic nature of the SST model allows us to track not only the fates of individual viral infection events (Figs. 2 and 3), but also of provirions and the associated fate transitions (Fig. 7). We selected all infection events that formed the provirion within 24 h.p.i. We sorted the infected cells based on their time to integration (TI). Many provirions disappeared after 12 h.p.i. due to death of the host cell, which also causes the drop of the population average (blue line). The individual fate transition dynamics of each cell that are not captured by the population average (Fig. 7) or by

the ODE model. The long distribution of the timing in the HIV infection are confirmed by single cell experimental data (Timm and Yin, 2012) and are relevant to pharmacological targeting at each steps (Murray et al., 2011).

In the context of viral infections, stochastic modeling approaches are critical in the context of low multiplicities of infection (MOI) (Srivastava et al., 2002). Under such condition, fluctuations in the levels of viral constituents can lead to qualitatively different behavior by rendering the system deterministically unstable when considering positive feedback mechanisms (Srivastava et al., 2002). Although the present model does not have such an unstable state, the low MOI condition applies and the SST model formulation demonstrates dynamic features that can only be captured by stochastic models. Thus the present model may function as an appropriate building block for modeling a larger scope of HIV infection dynamics at single cell resolution, and/or integration into immune response models, which often contain positive feedback amplification motifs.

Acknowledgments

Appendix A. Supplementary material

Supplementary data associated with this article can be found in the online version at http://dx.doi.org/10.1016/j.jtbi.2016.02.001.

References

Althaus, C.L., De Boer, R.J., 2010. Intracellular transactivation of HIV can account for the decelerating decay of virus load during drug therapy. Mol. Syst. Biol. 6, doi: ARTN 348 10.1038/msb.2010.4.

Anderson, J.L., Campbell, E.M., Wu, X.L., Vandegraaff, N., Engelman, A., Hope, T.J., 2006. Proteasome inhibition reveals that a functional preintegration complex intermediate can be generated during restriction by diverse TRIM5 proteins. J. Virol. 80, 9754–9760. http://dx.doi.org/10.1128/Jvi.01052 − 06.

Arhel, N., Genovesio, A., Kim, K.A., Miko, S., Perret, E., Olivo-Marin, J.C., Shorte, S., Charneau, P., 2006. Quantitative four-dimensional tracking of cytoplasmic and nuclear HIV − 1 complexes. Nat. Methods 3, 817–824, doi:nmeth928 [pii] 10.1038/nmeth928.

Arhel, N.J., Souquere-Besse, S., Munier, S., Souque, P., Guadagnini, S., Rutherford, S., Prevost, M.-C., Allen, T.D., Chameau, P., 2007. HIV − 1 DNA Flap formation promotes uncoating of the pre-integration complex at the nuclear pore. EMBO J. 26, 3025–3037. http://dx.doi.org/10.1038/sj.emboj.7601740.

Berger, E.A., Murphy, P.M., Farber, J.M., 1999. Chemokine receptors as HIV-1 coreceptors: roles in viral entry, tropism, and disease. Annu. Rev. Immunol. 17, 657–700, doi:Doi 10.1146/Annurev.Immunol.17.1.657.

Brandenburg, B., Zhuang, X., 2007. Virus trafficking – learning from single-virus tracking. Nat. Rev. Microbiol. 5, 197–208, doi:nrmicro1615 [pii] 10.1038/nrmicro1615.

Brussel, A., Sonigo, P., 2003. Analysis of early human immunodeficiency virus type 1 DNA synthesis by use of a new sensitive assay for quantifying integrated provirus. J. Virol. 77, 10119–10124.

Butler, S.L., Hansen, M.S., Bushman, F.D., 2001. A quantitative assay for HIV DNA integration in vivo. Nat. Med. 7, 631–634. http://dx.doi.org/10.1038/87979 87979 [pii].

Butler, S.L., Johnson, E.P., Bushman, F.D., 2002. Human immunodeficiency virus cDNA metabolism: notable stability of two-long terminal repeat circles. J. Virol. 76, 3739–3747.

Deng, N.J., Zheng, W., Gallicchio, E., Levy, R.M., 2011. Insights into the dynamics of HIV-1 protease: a kinetic network model constructed from atomistic simulations. J. Am. Chem. Soc. 133, 9387–9394. http://dx.doi.org/10.1021/ja2008032.

Dinh, A.T., Theofanous, T., Mitragotri, S., 2005. A model for intracellular trafficking of adenoviral vectors. Biophys. J. 89, 1574–1588. http://dx.doi.org/10.1529/Biophysj.105.059477.

Dinh, A.T., Pangarkar, C., Theofanous, T., Mitragotri, S., 2007. Understanding intracellular transport processes pertinent to synthetic gene delivery via stochastic

simulations and sensitivity analyses. Biophys. J. 92, 831–846. http://dx.doi.org/10.1529/Biophysj.106.095521.

Doranz, B.J., Baik, S.S.W., Doms, R.W., 1999. Use of a gp120 binding assay to dissect the requirements and kinetics of human immunodeficiency virus fusion events. J. Virol. 73, 10346–10358.

Gillespie, D.T., 1977. Exact stochastic simulation of coupled chemical-reactions. J. Phys. Chem. 81, 2340–2361. http://dx.doi.org/10.1021/J100540a008.

Haase, A.T., 2010. Targeting early infection to prevent $HIV-1$ mucosal transmission. Nature 464, 217–223. http://dx.doi.org/10.1038/nature08757.

Ho, D.D., Neumann, A.U., Perelson, A.S., Chen, W., Leonard, J.M., Markowitz, M., 1995. Rapid turnover of plasma virions and CD4 lymphocytes in HIV-1 infection. Nature 373, 123–126. http://dx.doi.org/10.1038/373123a0.

Hulme, A.E., Perez, O., Hope, T.J., 2011. Complementary assays reveal a relationship between HIV-1 uncoating and reverse transcription. Proc. Natl. Acad. Sci. USA 108, 9975–9980. http://dx.doi.org/10.1073/Pnas.1014522108.

Khalili, S., Armaou, A., 2008. Sensitivity analysis of HIV infection response to treatment via stochastic modeling. Chem. Eng. Sci. 63, 1330–1341. http://dx.doi.org/10.1016/J.Ces.2007.07.072.

Kim, H., Yin, J., 2005. In silico mutagenesis of RNA splicing in HIV-1. Biotechnol. Bioeng. 91, 877–893. http://dx.doi.org/10.1002/bit.20560.

McDonald, D., Vodicka, M.A., Lucero, G., Svitkina, T.M., Borisy, G.G., Emerman, M., Hope, T.J., 2002. Visualization of the intracellular behavior of HIV in living cells. J. Cell Biol. 159, 441–452. http://dx.doi.org/10.1083/Jcb.200203150.

Miyauchi, K., Kim, Y., Latinovic, O., Morozov, V., Melikyan, G.B., 2009. HIV enters cells via endocytosis and dynamin-dependent fusion with endosomes. Cell 137, 433–444. http://dx.doi.org/10.1016/j.cell.2009.02.046.

Mohammadi, P., Desfarges, S., Bartha, I., Joos, B., Zangger, N., Munoz, M., Gunthard, H.F., Beerenwinkel, N., Telenti, A., Ciuffi, A., 2013. 24 h in the life of HIV-1 in a T cell line. PLoS Pathog. 9, e1003161. http://dx.doi.org/10.1371/journal.ppat.1003161.

Murray, J.M., Kelleher, A.D., Cooper, D.A., 2011. Timing of the components of the HIV life cycle in productively infected CD4+T cells in a population of HIV-infected individuals. J. Virol. 85, 10798–10805. http://dx.doi.org/10.1128/JVI.05095−11.

Myszka, D.G., Sweet, R.W., Hensley, P., Brigham-Burke, M., Kwong, P.D., Hendrickson, W.A., Wyatt, R., Sodroski, J., Doyle, M.L., 2000. Energetics of the HIV gp120-CD4 binding reaction. Proc. Natl. Acad. Sci. USA 97, 9026–9031.

Perelson, A.S., 2002. Modelling viral and immune system dynamics. Nat. Rev. Immunol. 2, 28–36. http://dx.doi.org/10.1038/nri700.

Poncelet, P., Poinas, G., Corbeau, P., Devaux, C., Tubiana, N., Muloko, N., Tamalet, C., Chermann, J.C., Kourilsky, F., Sampol, J., 1991. Surface CD4 density remains constant on lymphocytes of HIV-infected patients in the progression of disease. Res. Immunol. 142, 291–298.

Raviv, Y., Viard, M., Bess, J., Blumenthal, R., 2002. Quantitative measurement of fusion of HIV-1 and SIV with cultured cells using photosensitized labeling. Virology 293, 243–251. http://dx.doi.org/10.1006/Viro.2001.1237.

Reddy, B., Yin, J., 1999. Quantitative intracellular kinetics of HIV type 1. AIDS Res. Hum. Retrovir. 15, 273–283. http://dx.doi.org/10.1089/088922299311457.

Reynes, J., Portales, P., Segondy, M., Baillat, V., Andre, P., Reant, B., Avinens, O., Couderc, G., Benkirane, M., Clot, J., Eliaou, J.F., Corbeau, P., 2000. CD4+T cell surface CCR5 density as a determining factor of virus load in persons infected with human immunodeficiency virus type 1. J. Infect. Dis. 181, 927–932. http://dx.doi.org/10.1086/315315.

Srivastava, R., You, L., Summers, J., Yin, J., 2002. Stochastic vs. deterministic modeling of intracellular viral kinetics. J. Theor. Biol. 218, 309–321.

Stein, B.S., Gowda, S.D., Lifson, J.D., Penhallow, R.C., Bensch, K.G., Engleman, E.G., 1987. Ph-Independent Hiv Entry into Cd4-Positive T-Cells Via Virus Envelope Fusion to the Plasma-Membrane. Cell 49, 659–668. http://dx.doi.org/10.1016/$0092-8674(87)90542-3$.

Stelling, J., Gilles, E.D., Doyle 3rd, F.J., 2004. Robustness properties of circadian clock architectures. Proc. Natl. Acad. Sci. USA 101, 13210–13215. http://dx.doi.org/10.1073/pnas.0401463101.

Timm, A., Yin, J., 2012. Kinetics of virus production from single cells. Virology 424, 11–17. http://dx.doi.org/10.1016/j.virol.2011.12.005.

Weinberger, L.S., Burnett, J.C., Toettcher, J.E., Arkin, A.P., Schaffer, D.V., 2005. Stochastic gene expression in a lentiviral positive-feedback loop: $HIV-1$ Tat fluctuations drive phenotypic diversity. Cell 122, 169–182, doi:$S0092-8674(05)00549-0$ [pii] 10.1016/j.cell.2005.06.006.